

Data Assimilation using Bayesian Filters and B-spline Geological Models

Lian Duan¹, Chris Farmer¹, Ibrahim Hoteit², Xiaodong Luo², Irene Moroz³

¹ Oxford Centre for Collaborative Applied Mathematics, Mathematical Institute, University of Oxford, 24 - 29 St Giles, Oxford, OX1 3LB

² King Abdullah University of Science and Technology, Thuwal, Saudi Arabia

³ Oxford Centre for Industrial and Applied Mathematics, Mathematical Institute, University of Oxford, 24 - 29 St Giles, Oxford, OX1 3LB

E-mail: lian.duan@maths.ox.ac.uk

Abstract. This paper proposes a new approach to problems of data assimilation, also known as history matching, of oilfield production data by adjustment of the location and sharpness of patterns of geological facies. Traditionally, this problem has been addressed using gradient based approaches with a level set parameterization of the geology. Gradient-based methods are robust, but computationally demanding with real-world reservoir problems and insufficient for reservoir management uncertainty assessment. Recently, the ensemble filter approach has been used to tackle this problem because of its high efficiency from the standpoint of implementation, computational cost, and performance. Incorporation of level set parameterization in this approach could further deal with the lack of differentiability with respect to facies type, but its practical implementation is based on some assumptions that are not easily satisfied in real problems.

In this work, we propose to describe the geometry of the permeability field using B-spline curves. This transforms history matching of the discrete facies type to the estimation of continuous B-spline control points. As filtering scheme, we use the ensemble square-root filter (EnSRF). The efficacy of the EnSRF with the B-spline parameterization is investigated through three numerical experiments, in which the reservoir contains a curved channel, a disconnected channel or a 2-dimensional closed feature. It is found that the application of the proposed method to the problem of adjusting facies edges to match production data is relatively straightforward and provides statistical estimates of the distribution of geological facies and of the state of the reservoir.

1. Introduction

History matching is the art of adjusting reservoir models until they reproduce the past reservoir behaviour, consisting of historical production and pressure data. Once a model has been history matched, it is often assumed that it can then be used to simulate future reservoir behaviour with a higher degree of confidence, particularly if the adjustments are constrained by known geological properties in the reservoir [1]. However, it can be shown within the Bayesian framework that such history matched models are modes of the posterior density and by using an over-smoothed model that may only be a local maximum of the posterior density there are no reasons whatever for assuming that history matched models have any particular predictive power. Only by adopting a fully Bayesian approach one can hope to quantify the uncertainty in the history matched models

and then only if the equations used to model the reservoir are a faithful representation of the reservoir physics.

Before automatic history matching of realistic reservoir models became feasible, reservoir models were history matched manually using engineering judgement and a work flow that has developed through years of experience (such as in [2]). However, such a procedure can be efficient only when a small number of parameters needs to be retrieved from the observed production data. It took Agarwal *et al.* [3] one year of intensive work to match 25 years worth of production and performance data for a complex fractured chalk reservoir in the Norwegian North Sea, with 76 production wells, 13 gas injectors and 37 water injectors.

Automatic strategies for history matching were initially based on the perturbation method. This method computes the single grid block sensitivity coefficients in order to evaluate the change of an objective function to small perturbations of the permeability field [4, 5]. For every iteration, the direct method of computing these sensitivity coefficients requires integrating the reservoir model as many times as the number of parameters to be determined. In consequence, this approach is computationally quite demanding for real reservoir history matching problems. Later methods used adjoint techniques which can be very efficient, but are very difficult to code. Nowadays, advanced automatic strategies are statistical and are based on the Ensemble Kalman filter (EnKF) approach [6, 7] and sometimes the method of randomised maximum likelihood [8, 9, 10] which does use adjoint methods [11]. EnKF methods build the solution sequentially every time a new observation is available by updating the mean and the posterior correlation matrix, while deterministic variational methods produce maximum-likelihood solutions through minimization of an objective function.

Given the limited amount of data and the complexity of the problem, many engineers prefer to adjust relatively small numbers of parameters (“global parameters”), even if the history matching problem is formulated as an automated process. For instance, large scale permeability trends, like barriers and channels, have a large impact on how the fluid flows in a porous medium. Reliable knowledge of these geological structures is therefore important for the reservoir engineers controlling the production in the reservoir. One can then turn the history matching problem into an estimation problem of the geological facies pattern [12].

In geology, facies are a body of rock with specified characteristics such as permeability, porosity, etc[13]. In the existing literature, the history matching problem of the facies pattern has been addressed using a level set parameterization of the facies pattern with the parameters estimated as the solution of a gradient-based variational problem. The piecewise constant level set method [14] has been applied to many areas since the original method was introduced by Osher and Sethian [15, 16], e.g. for tracing interfaces between different phases [17], for image segmentation [18], or for optimal shape design problems [19].

Nielsen *et al.* [20] and Dorn *et al.* [21] applied the level set method to model the facies bodies and history matched the observed data of several synthetic reservoir models by minimising a misfit function between the simulated and observed data. This approach was found to be robust. However, it can be more computationally expensive for realistic problems than, say an EnKF method, because it requires integrating the adjoint of the model to determine the gradient descent minimization directions. More importantly, this method only provides a deterministic estimation without any information about the associated uncertainty, which might be insufficient for reservoir management.

Sequential ensemble-based data assimilation techniques, based on the work of the Ensemble Kalman Filter (EnKF) of [6, 7], appear to offer attractive features and powerful capabilities for the automatic history matching problem of facies pattern. The EnKF actually provides an efficient approach to estimate a large number of variables and is based on a simple conceptual formulation and relative ease of implementation (it does not need the linearization of the reservoir model nor the development of its adjoint and only requires forward integrations of the forward

reservoir model). It furthermore computes estimates of the solution uncertainties as part of its algorithm at reasonable computational cost.

The EnKF originated as a variant of the Kalman filter designed for large dimensional nonlinear systems and is now one of the most used data assimilation schemes. The filter propagates an ensemble of prior realizations with the nonlinear model and uses the linear Kalman filter correction step to update the ensemble every time new observations are available. Despite the underlying nature of its linear analysis step, the efficiency of EnKF method was demonstrated on different applications and in many situations achieved accurate estimation much faster than fully nonlinear Bayesian methods such as the particle filter [22]. The original formulation of the EnKF requires perturbing the observations so that its analysis covariance stochastically matches that of the Kalman filter. This might however introduce noise in the estimation process especially when the size of the ensemble is not much larger than the number of observations. The Ensemble Square Root Filter (EnSRF) was introduced as an alternative ensemble implementation that exactly matches the analysis covariance of the Kalman filter [23].

Because ensemble and other Kalman-based filters are only designed for the estimation of continuous variables, the main challenge in applying an EnKF to the history matching problem of the geological facies pattern is to transform the discrete facies variables into continuous variables through an appropriate parameterization of the facies.

Liu *et al.* [24, 25] used a threshold truncation map to describe the geostatistical model of the problem of interest, transforming the problem into a position estimation problem in each cell. The initial ensemble was generated using truncated pluri-Gaussian models. Very recently, Chang [26] combined the level set method and the traditional EnKF, naturally transforming the discrete facies variable of -1 and 1 to a continuous variable of real numbers less than or greater than 0 . Their initial ensemble was generated using multipoint geostatistics methods, such that the facies in each cell of the initial ensemble are centered and with a standard deviation of 0.5 . After the history matching process, the mean of the artificial facies values are corrected towards one side of zero with reduced uncertainty. Both schemes are however difficult to apply to a real reservoir problem because their assumptions for generating the initial ensemble are not often satisfied in real history matching problems.

In this paper, we introduce a new method to incorporate the level set method in an EnKF. The idea is based on a B-spline parameterization of the facies pattern. B-splines were introduced more than 50 years ago. The method is mainly used for curve fitting [27] and image registration [28]. It has been also applied in many other areas, such as neural networks [29] and cardiac motion estimation [30]. As in [20], our method used a binary level set function to represent the permeability field. The discontinuous curves of the level set functions are then parameterized by either two one-dimensional unclamped cubic B-splines for the channel features, or one two-dimensional clamped cubic B-spline for the two-dimensional closed features. Using this continuous parameterization of the edges of the facies, we will demonstrate that the history matching problem of the facies pattern can be solved using the EnSRF.

The paper is organised as follows. Section 2 presents the reservoir model and describes the history matching problem and its state-space formulation. The EnSRF which is used to solve the history matching problem is summarised in Section 3. The general framework for level set modelling is presented in Section 4. An introduction of the B-spline parameterizations for the discontinuous curve of the level set functions is presented in Section 5. Section 6 discusses the key B-spline parameterizations and the typical form of filter realizations. Section 7 presents and discusses the results of three different numerical experiments of facies pattern history matching problems. A summary and a discussion conclude the work in Section 8.

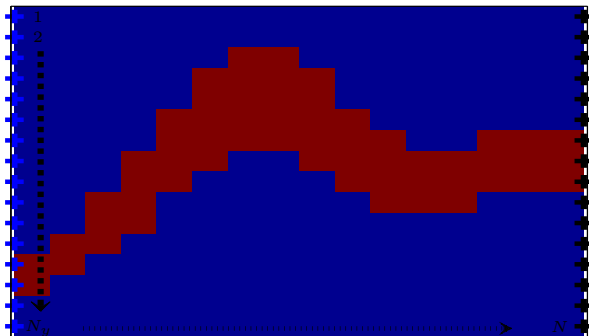


Figure 1. The facies of the reservoir model, blue cells (shale), red cells (sandstone), blue pluses (injectors) and black pluses (producers).

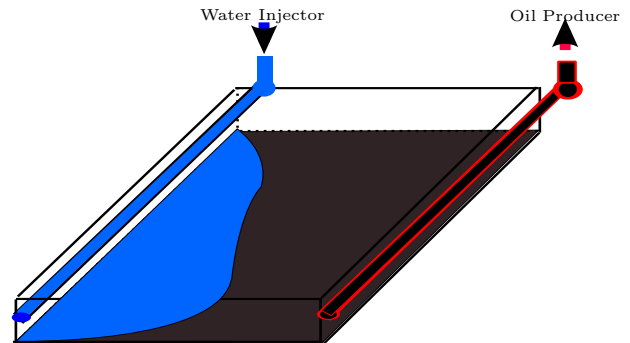


Figure 2. Three-dimensional view of the oil enhanced recovery using water flooding experiment as presented in [31].

2. Reservoir Model and History Matching Problem

We consider a two dimensional horizontal rectangular reservoir model with isotropic permeability and assume that it is fully saturated with water and oil initially (as shown in Fig. 1). The reservoir is formed by two types of rock, the large shale area with low permeability κ_l and a small amount of sandstone with high permeability κ_h . Using the water flooding experiment in [31], secondary oil recovery is performed by injecting water on the left boundary of the reservoir with a constant injection rate and producing oil from the right boundary of the reservoir with a constant bottom-hole pressure as shown in Fig. 2. Assuming incompressibility and immiscibility of the fluids, the model equations are the conservation of mass equations:

$$\phi(\underline{x}) \frac{\partial S_o}{\partial t} - \nabla \cdot \left(\frac{\kappa(\underline{x}) \kappa_{ro}(S_o)}{\mu_o} \nabla p_o \right) = q_o(\underline{x}), \quad (1)$$

$$\phi(\underline{x}) \frac{\partial S_w}{\partial t} - \nabla \cdot \left(\frac{\kappa(\underline{x}) \kappa_{rw}(S_w)}{\mu_w} \nabla p_w \right) = q_w(\underline{x}), \quad (2)$$

where $(\underline{x}, t) \in \Omega \times [0, T]$, $\Omega \subset \mathcal{R}^2$ is the bounded reservoir domain. Here, the subscripts o and w refer to the phases, oil and water, respectively. Also S_f denotes the saturation, μ_f the viscosity, p_f the pressure, q_f the external volumetric flow rate and κ_{rf} is the relative permeability, where f is the fluid phase. The porosity and the absolute permeability are given by $\phi(\underline{x})$ and $\kappa(\underline{x})$, respectively. Closure of the system is obtained through the assumption of a completely saturated medium, such that

$$S_o + S_w = 1, \quad (3)$$

and a function P_c defining the capillary pressure,

$$p_o - p_w = P_c. \quad (4)$$

The quantities $\phi, \kappa, \kappa_{rf}$ and P_c are all properties of the porous medium and are not accessible through direct measurements except at the wells. In the forward problem, they are assumed to be known such that the reservoir behaviour (ie. pressure and saturation of each fluid phrase) can be predicted using a finite volume simulator. In the history matching problem, these rock properties are the unknowns. More specifically, with some prior knowledge about the reservoir $\phi, \kappa_{rf}, \kappa$ values, the existence of features (ie. a channel or a close feature) and the rock properties along the left and right boundaries, our goal, in this paper, is to estimate the geological facies pattern

(hence the absolute permeability $\kappa(\underline{x})$) to predict the reservoir future behaviour conditioned upon pressure and water saturation measurements in the production well.

In the forward problem (or the reservoir simulator), the finite volume method is employed to discretize the reservoir domain Ω into $N = N_y \times N_x$ uniform spatial cells, where the variables within each cell are assumed constant. Equations (1, 2, 3, 4) are solved using a custom finite volume simulator, in which cell residuals are minimised implicitly in time by applying Newton iterations and the generalized minimal residual method (GMRES) as the linear solver. The cell index from top to bottom and then from left to right is denoted by superscript j from 1 to N as shown in Fig. 1. A typical (input) state vector x consists of state variables ($\mathbf{P} \in \mathcal{R}^{N \times 1}, \mathbf{S} \in \mathcal{R}^{N \times 1}$) and model parameters ($\mathbf{m} \in \mathcal{R}^{n_m \times 1}$), as follows:

$$x = \{\mathbf{P}, \mathbf{S}, \mathbf{m}\}^T = \{P^1, \dots, P^N, S^1, \dots, S^N, \mathbf{m}\}^T \in \mathcal{R}^{(2N+n_m) \times 1}. \quad (5)$$

with the superscript T denoting a matrix transpose. In each cell j , S^j is the water saturation and assuming a zero capillary pressure $P_c = 0$, the pressure for each fluid phase is

$$P^j = p_o^j = p_w^j. \quad (6)$$

The model parameters \mathbf{m} are time-independent variables and include unknown rock properties (such as the permeability and porosity fields). The choice of \mathbf{m} will be discussed in detail in Sections 4, 5 and 6.

In the history matching problem, the simulation of the pressure and saturation in every cell and the production data in the wells can be described using the state-space equations as follows:

$$x_k = f(x_{k-1}), \quad (7a)$$

$$s_k = Hx_k + v_k. \quad (7b)$$

Here, the subscript k is the time index; the function $f(\cdot)$ denotes the reservoir simulator and H is a $(2N_y) \times (2N + n_m)$ measurement matrix relating the state vector to the observations. In the present study it is of the form

$$H = \begin{pmatrix} I^{N_y} & 0 & 0 & 0 \\ \underbrace{0}_{N_y} & \underbrace{0}_{2N - 2N_y} & \underbrace{I^{N_y}}_{N_y} & \underbrace{0}_{n_m} \end{pmatrix}, \quad (8)$$

where the matrix I^{N_y} is an $N_y \times N_y$ identity matrix. The first and second matrices I^{N_y} take the measurements on the pressure in the injection wells and water saturation in the production wells, respectively. The measurement noise v_k is modelled here as an independent multivariate Gaussian distribution with mean 0 and covariance matrix

$$R = \begin{pmatrix} \sigma_P^2 I^{N_y} & 0 \\ 0 & \sigma_S^2 I^{N_y} \end{pmatrix}, \quad (9)$$

where σ_P and σ_S are respectively the standard deviation of the pressure measurement noise in the injection wells and the water saturation measurement in the production wells.

3. Ensemble Square Root Filter (EnSRF)

The Ensemble Square Root Filter (EnSRF) is an ensemble Kalman filter suitable for large-scale nonlinear models. It was introduced by [23] to avoid the noise introduced by the perturbed observation needed in the original EnKF. At time t_k , it provides estimates of the state vector

X_k and the associated uncertainty based on an ensemble of r realizations from the distribution of the state denoted by

$$X_k = \{x_{k,1}, x_{k,2}, \dots, x_{k,i}, \dots, x_{k,r}\} \in \mathcal{R}^{(2N+n_m) \times r}. \quad (10)$$

Here, the subscript $i \in [0, r]$ denote the realization index and each realization $x_{k,i} \in \mathcal{R}^{(2N+n_m) \times 1}$ consists of state variables and model parameters, as in equation (5):

$$x_{k,i} = \{P_{k,i}^1, \dots, P_{k,i}^N, S_{k,i}^1, \dots, S_{k,i}^N, \mathbf{m}_{k,i}\}^T \in \mathcal{R}^{(2N+n_m) \times 1}, \quad (11)$$

Following these definitions and notations, the algorithm of the EnSRF can be summarized as an initialization step, a sequence of forecast steps (with the model to update the ensemble forward in time) followed each time by an analysis step to update the forecast ensemble conditioned on the new observations. After a prediction or an analysis step, the state estimate is taken as the mean and the associated uncertainty is represented by the ensemble sample covariance matrix.

Initialization step:

- (i) The probability density function $\pi(\mathbf{P}_0, \mathbf{S}_0, \mathbf{m})$ of the initial state and model parameters is assumed to be given and is represented statistically by an ensemble $X_0^a = \{x_{0,1}^a, \dots, x_{0,r}^a\}$.
- (ii) For every filtering step $k = 1, 2, \dots$, proceed as follows;

Forecasting step

- (a) Integrate the available analysis ensemble $X_k^a = \{x_{k,1}^a, \dots, x_{k,r}^a\}$ forward with the nonlinear reservoir model (7a) to the time of the next available observation to compute the forecast ensemble $X_k^f = \{x_{k,1}^f, \dots, x_{k,r}^f\}$ as

$$x_{k,i}^f = f(x_{k-1,i}^a) \quad \text{for } i = 1, \dots, r, \quad (12)$$

where the superscripts f and a denote forecast and analysis, respectively.

- (b) Compute the forecast state \hat{x}_k^f , the forecast ensemble anomalies $A_k^f = [A_{k,1}^f, \dots, A_{k,r}^f]$:

$$\hat{x}_k^f = \frac{1}{r} \sum_{i=1}^r x_{k,i}^f, \quad (13)$$

$$A_{k,i}^f = \frac{1}{\sqrt{r-1}} (x_{k,i}^f - \hat{x}_k^f). \quad (14)$$

The forecast error covariance matrix is then

$$P_k^f = A_k^f (A_k^f)^T, \quad (15)$$

but does not need to be explicitly computed for the filter algorithm.

Analysis step

- (c) Compute the Kalman Gain Matrix K_k :

$$K_k = P_k^f H^T (H P_k^f H^T + R)^{-1}. \quad (16)$$

- (d) Calculate the analysis \hat{x}_k^a by using the Kalman analysis equation:

$$\hat{x}_k^a = \hat{x}_k^f + K_k (s_k - H_k \hat{x}_k^f). \quad (17)$$

- (e) Perform an eigenvalue decomposition on $(I - K_k H)$, such that $(I - K_k H) = U D U^{-1}$ with positive eigenvalues only, $D_{ii} > 0$.
- (f) Generate a new analysis ensemble X_k^a using a transform matrix T and the previous ensemble anomalies A_k^a as:

$$T = U D^{1/2} U, \quad (18a)$$

$$A_k^a = T A_k^f, \quad (18b)$$

$$X_k^a = \hat{x}_k^a \cdot \mathcal{U}^{1 \times r} + \sqrt{r-1} A_k^a, \quad (18c)$$

where $\mathcal{U}^{1 \times r}$ denotes a $1 \times r$ unit matrix (matrix of 1s).

4. Level Set Modelling of the Permeability Field

With the aim of estimating the facies pattern, hence the permeability field, it is natural to consider the vector of facies as the parameter vector \mathbf{m} to be estimated with the ensemble Kalman filter in the history matching problem [32]. Using prior knowledge about the existence of features (ie. a channel or a closed feature) and two types of rocks with absolute permeability κ_h and κ_l in the reservoir, one can model the facies pattern and absolute permeability field using level set functions.

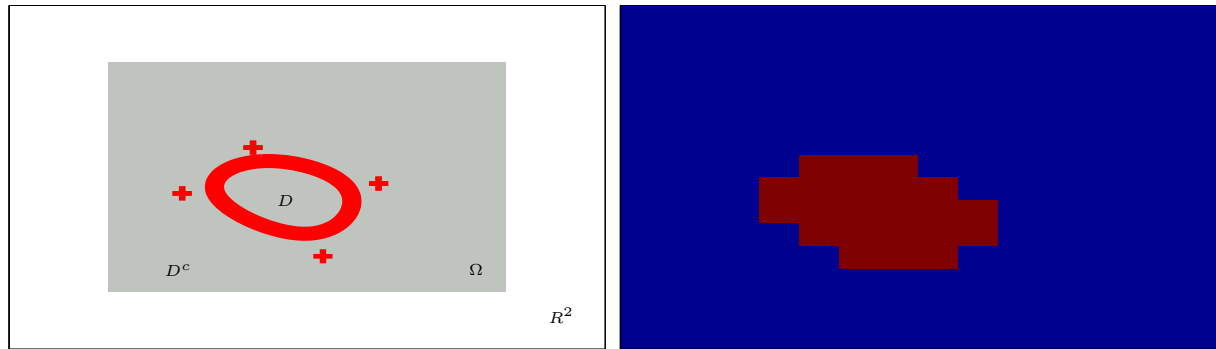


Figure 3. Permeability field with a two-dimensional closed feature modelled by a level set function via B-spline parameterization of the discontinuous curve. Plots show the reservoir domain Ω (gray rectangle), the B-spline control point domain (outer white rectangle bounded by black edges), discontinuous curve of the level set function (left figure in red), B-spline control points (left figure red pluses) and the corresponding permeability field (right figure) using equations (19) and (20).

Level set functions are discontinuous functions which at convergence take the values 1 and -1 inside and outside two subregions. If a domain Ω is divided into two subregions, D and D^c ($D^c = \Omega \setminus D$ is the complement of D), a level set function Φ is defined as:

$$\Phi(\underline{x}) = 1, \quad \forall \underline{x} \text{ in } D, \quad \Phi(\underline{x}) = -1, \quad \forall \underline{x} \text{ in } D^c. \quad (19)$$

The curve separating D and D^c representing the edges of the sandstone is implicitly given as the discontinuous curve ς of Φ . The properties of Φ can be used to construct the facies pattern and the permeability field $\kappa(\underline{x})$ with distinct constant values inside the two different subdomains. The facies variable in each cell is modelled as a discrete variable taking value of -1 or 1 . As in Fig. 3, if we assume that the value of $\kappa(\underline{x})$ is equal to κ_h in D and equal to κ_l in D^c , the $\kappa(\underline{x})$ can be written as

$$\kappa(\underline{x}) = \frac{1}{2} [\kappa_h (\Phi(\underline{x}) + 1) - \kappa_l (\Phi(\underline{x}) - 1)], \quad (20)$$

with constraints

$$\Phi(\underline{x})^2 - 1 = 0. \quad (21)$$

5. B-spline Parameterization

Estimating the facies type of each cell by including these as parameters in the EnSRF state vector is not compatible with the formulation of the filter. Indeed, Kalman type ensemble filters are designed to work with continuous variables while the facies type is a discrete variable taking one of two values -1 or 1 (or κ_h or κ_l for permeability field) only. Even if the filter starts with a forecast ensemble consisting of two types of rocks, the updated ensemble will not necessarily consist of the same type of rocks after the analysis step. This is the biggest challenge of using an ensemble-based Kalman filter for the history matching of facies in a reservoir.

To go around this problem and use an ensemble filter for the estimation of facies patterns, one needs to introduce a parameterization that transforms the discrete variables representing the facies (or permeability) into continuous variables [24, 25, 26] and then use the latter in the estimation process. In this paper, this is achieved by parameterizing the discontinuous curve ς of the level set function using B-spline functions. These are designed around local control points with global smoothness constraints making them particularly useful for our problem [33].

The idea of the B-spline method is briefly recalled hereafter. The reader is referred to [33] for a detailed description of the method. A B-spline is a spline function that has minimal support with respect to a given degree, smoothness and domain partition. It is a generalisation of a Bézier curve. The definition of a two-dimensional uniform unclamped B-spline approximation that can be summarized as follows:

$$\varsigma(\chi) = \sum_{c=0}^n N_{c,d}(\tau) \underline{b}^c. \quad (22a)$$

The subscript $c \in [0, n]$ is the index of the control point; the subscript d is the degree of the curve; $\chi \in [0, 1]$ is an evaluation point; $\underline{b}^c = (a^c, b^c) \in \mathcal{R}^2$ are the $n + 1$ control points, where a^c is along the direction perpendicular to the left boundary of the reservoir with 0 at the left boundary, and b^c is along the direction horizontal to the left boundary of the reservoir with 0 at the top boundary. The $N_{c,d}(\chi)$ are the B-spline basis functions and are recursively constructed as a function of $n + d + 1$ knots χ_m . The knots χ_m are constructed in the standard open uniform fashion, as follows:

$$\chi_m = \begin{cases} 0, & 0 \leq m \leq d \\ \frac{m-d}{n+1-d}, & d+1 \leq m \leq n \\ 1, & n+1 \leq m \leq n+d+1 \end{cases}. \quad (22b)$$

The recursive definition of the B-spline functions starts from the basis function

$$N_{c,d}(\chi) = \begin{cases} 1, & \chi_c \leq \chi \leq \chi_{c+1} \\ 0, & \text{otherwise} \end{cases} \quad (22c)$$

for $0 \leq c \leq n + d$. The functions are then computed recursively as

$$N_{c,l}(\chi) = \frac{\chi - \chi_c}{\chi_{c+l} - \chi_c} N_{c,l-1}(\chi) + \frac{\chi_{c+l+1} - \chi}{\chi_{c+l+1} - \chi_{c+1}} N_{c+1,l-1}(\chi) \quad (23)$$

for $1 \leq l \leq d$ and $0 \leq c \leq n + d - l$. The support of any B-spline function $N_{c,l}(\chi)$ is then $[\chi_c, \chi_{c+l+1}]$.

For parameterizing closed curves, it is advisable to use the clamped B-splines. These are computed using wrapping control points (or joining the ends) and a degree d B-spline with $n + 1$ control points which can be generated in the following way:

- (i) Generate d fictitious control points $\{\underline{b}^{n+1}, \dots, \underline{b}^{n+d}\}$ such that:

$$\underline{b}^{n+1} = \underline{b}^1, \quad \underline{b}^{n+2} = \underline{b}^2, \quad \dots, \quad \underline{b}^{n+d} = \underline{b}^d. \quad (24)$$

The number of control points is artificially increased from $n + 1$ to $n + d + 1$. The index of the control point is now between 0 to \tilde{n} , where $\tilde{n} = n + d$.

- (ii) By replacing n by \tilde{n} , the clamped B-splines is generated using equation (22a) with basis function in equations (22c, d) and uniform knots (22b).

6. Updating Facies Patterns with EnSRF

Let us first consider a reservoir with a channel feature. The discontinuous curve ς of the level set function is then parameterized by two one-dimensional unclamped B-splines. Although the control points $\underline{b}^c = (a^c, b^c)$ are two-dimensional, they are located uniformly along the direction perpendicular to the left boundary of the reservoir with fixed a^c s. Assuming prior knowledge of the existence of a facies feature and the rock properties along the left and right boundaries, the upper edge of the discontinuous curve ς (or the channel) is parameterized by a one-dimensional unclamped B-spline function with fixed starting and ending control points and $n + 1$ intermediate control points $\{b^0, b^1, \dots, b^n\}$, as shown in Fig. 4. Similarly, we consider $n + 1$ intermediate control points $\{b^{n+1}, \dots, b^{2n+1}\}$ to parameterize the lower edge of the discontinuous curve. It is noted that the control points are continuous variables in R^2 , which contains the reservoir domain Ω and the region where the upper edge of the discontinuous curve ς below the lower edge is assumed to be contained in D^c . The model parameters to be included as part of the the filter state vector will therefore consist of the positions of the intermediate control points. A typical realization of the ensemble of the EnSRF will therefore be of the form:

$$x_{k,i} = \{P_{k,i}^1, \dots, P_{k,i}^N, S_{k,i}^1, \dots, S_{k,i}^N, b_{k,i}^0, \dots, b_{k,i}^{2n+1}\}^T. \quad (25)$$

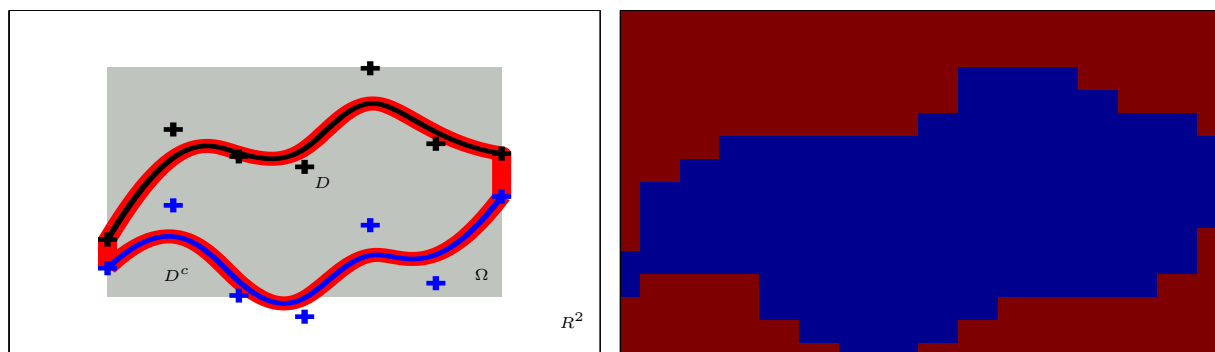


Figure 4. Permeability field featuring a channel modelled by a level set function via B-spline parameterization of the discontinuous curve. Plots show the reservoir domain Ω (gray rectangle), the B-spline control point domain (outer white rectangle bounded by black edges), discontinuous curve of the level set function (left figure in red), B-spline control points (left figure black pluses) for the upper edge of the discontinuous curve (left figure in black), B-spline control points (left figure blue pluses) for the lower edge of the discontinuous curve (left figure in blue), and the discontinuous curve of the level set function (left figure in red) and the corresponding permeability field (right figure) computed using equations (19) and (20).

For a reservoir with two-dimensional closed features, as in Fig. 3, the curve ς of the level set function is parameterized by a two-dimensional clamped B-spline. The model parameters to be

included in the state vector will be the values of the $n + 1$ control points. In this case, typical realization of the ensemble of the EnSRF will be of the form:

$$x_{k,i} = \{P_{k,i}^1, \dots, P_{k,i}^N, S_{k,i}^1, \dots, S_{k,i}^N, a_{k,i}^0, \dots, a_{k,i}^n, b_{k,i}^0, \dots, b_{k,i}^n\}^T. \quad (26)$$

The estimation process we are dealing with is greatly complicated by the nature of the geological heterogeneity, which is not amenable to simple parameter descriptions. One may always consider a large enough number of control points to allow for more flexibility to reproduce the complicated spatial configuration. This might however make the estimation problem of the facies pattern more difficult because it increases the chances of having different parameter sets producing comparable fits to the available measurements [11, 34, 35]. In this case, it would be more appropriate to constrain the number of control points which could lead to a lower-dimensional estimation problem but at the price of missing some features of the true reservoir geometry. In this work, we choose $n = 4$ for reservoirs with channel features and $n = 3$ for reservoirs with two-dimensional closed features.

7. Numerical Experiments

Three numerical experiments were performed to test the proposed method and to evaluate its performance. More specifically, the EnSRF was used to estimate the facies patterns of three different permeability fields using synthetic pressure and saturation measurements. Facies patterns were parameterized using B-splines as described in section 6. In these experiments, the true permeability field consists of two distinct values and the test cases are a curved channel (Fig. 5), a disconnected channel (Fig. 7), and a two-dimensional closed feature (Fig. 10). The reservoir is square and horizontal with constant thickness and non-flow outer boundary. The relative permeability functions are defined by the Corey models:

$$\begin{aligned} \kappa_{rw} &= \hat{\kappa}_{rw} \left(\frac{S_w - S_{wr}}{1 - S_{wr} - S_{or}} \right)^{e_w}, \\ \kappa_{ro} &= \hat{\kappa}_{ro} \left(\frac{S_o - S_{or}}{1 - S_{or} - S_{wr}} \right)^{e_o}. \end{aligned}$$

where the Corey exponents, e_w and e_o , the residual saturations, S_{wr} and S_{wo} , and the endpoint permeabilities, $\hat{\kappa}_{rw}$ and $\hat{\kappa}_{ro}$, are assumed to be known. The numerical values of the reservoir properties are listed in table 1.

For each reference permeability field we simulate the ‘true’ values of saturation (S_w) and pressure (p_w) for the applied time steps on the given grid by integrating the reservoir model forward in time. Synthetic measurements are then extracted from the true states and perturbed with random noise to test the system in the Prefect Model Scenario (PMS). The measurement noise is assumed to be uncorrelated Gaussian noise with zero mean. The standard deviation of the pressure measurement noise in the injector wells and the water saturation measurement in the projection wells are $\sigma_P = 2$ bar and $\sigma_S = 0.002$, respectively. The automatic history matching of the facies pattern is then performed by assimilating these measurements every 16 days and over an 800 day period. The estimated permeability field is then used to predict the reservoir behaviour from day 801 to day 1600. To mitigate the problem of ensemble collapse, large ensembles with $r = 600$ members were used in the experiments. The mean of the ensemble pressure and saturation are taken as the estimated pressure and saturation in the cells, respectively. In all experiments cubic B-splines were used.

We use two different approaches for the estimation of log permeability fields:

- (i) *Calculate the log permeability field from the mean of the B-spline control points (LPMB):*
The discontinuous curve ς of the level set function is first computed from the mean of the

Reservoir dimensions:	$1000m \times 1000m \times 40m$	
Simulation grid:	$16 \times 16 \times 1$ cells	
Porosity:	0.2	
Viscosity:	$\mu_w = 0.5 \cdot 10^{-3}$ Pa.s	$\mu_o = 0.5 \cdot 10^{-3}$ Pa.s
Endpoint relative permeability:	$\hat{\kappa}_{rw} = 0.1$	$\hat{\kappa}_{ro} = 1$
Residual saturations:	$S_{wr} = 0.2$	$S_{or} = 0.2$
Corey exponents:	$e_w = 2$	$e_o = 3$
Initial saturations:	$S_w = 0.2$	$S_o = 0.8$
Capillary pressure function:	$P_c(S_w) \equiv 0$ kPa	
Injector rate:	8% of total pore volume per year	
Production rate:	constant BHP= 200.0 bar	
Number of timesteps:	100	
Total production time:	1600 days	

Table 1. Key properties in the reservoir simulator

analysed ensemble. The log permeability field is then obtained using equations (19 and 20). The LPMB figures consist of the same number of rock types as the reference permeability field and will be used for the comparison against the reference field.

- (ii) *Take the mean of the log permeability fields computed from each set of the B-spline control points (MLP):* The log permeability fields associated with the B-spline parameterization of the discontinuous curve ς in each realization of the analysed ensemble are first calculated. The estimated log permeability field is then found by averaging the log permeability fields cell-by-cell. During this process, artificial rock types might be generated. The MLP figures will be used to evaluate the quality of the estimated permeability field during the history matching period. The standard deviation of the log permeability field (SDLP) estimated from the realizations of the B-spline control points of the analysed ensemble is also used as a measure of the uncertainty about the estimated permeability.

To evaluate the estimates of the facies pattern, we present figures plotting the discontinuous curve of the reference permeability field, the estimated discontinuous curve, and the cells with large facies uncertainty. The estimated discontinuous curve is further plotted along the boundary of the cells where a sign change occurs in the mean level set function. We define the cells with facies standard deviation greater than 0.8 as the cells with large facies uncertainty, and label these in black dots in their corresponding cell centers.

7.1. Curved and Disconnected Channels

In the case the permeability field has a curved channel or a disconnected channel, a typical realization of the state vector in the EnSRF will be of the same form as equation (25).

Fig. 5 presents the evolutions of the log permeability field and the facies patterns estimates with the corresponding uncertainties over the history matching period for the curved channel case. The true log permeability field is plotted in the top panel, where the location and index of the injection and production wells are labelled by blue and black pluses, respectively. The time-evolution of the log permeability fields as estimated by the mean of the B-spline control points (LPMB) is plotted in the second row, the mean (MLP) and standard deviation (SDLP) of the log permeability field are plotted in the third and fourth row, respectively; and figures comparing the true and estimated discontinuous curves, and indicating the cells with large facies uncertainty are plotted in the fifth row.

Because of the lack of complete knowledge of the initial state of the reservoir (on day 0) in

realistic applications, the initial realizations of the EnSRF are considered to be quite different from the true reservoir permeability field and facies pattern. One can see from Fig. 5 that the convergence toward the true permeability field is rather slow and after 192 assimilation days (12 assimilation cycles) the facies estimates are still quite different from the true facies. This is due to the limited amount of information (observation) that have been used in the estimation process. The filter however preserves standard deviations indicating large uncertainties on the estimates during that period. As more information become available over time, the estimation of the permeability field and facies pattern gradually improves. At the end of the history matching period, the estimated permeability field and facies pattern are almost identical to the true fields. Only one cell is showing a significant mismatch between the estimated and the true permeability, but the truth lies within the estimated uncertainty.

Fig. 6 shows typical data assimilation processes in an injection well (no. 7), and three production wells (no. 3, 14 and 16) over time. The true states are plotted in red, the measurements are plotted in blue, the simulations of the initial ensembles are plotted in magenta, and the EnSRF ensembles at the end of each analysis steps are plotted in green. One can see that the history matching of the pressure in the injection well and saturation in the production wells have been very well reproduced. The uncertainty level (the vertical width of the green lines) provided by the EnSRF which is much smaller than the initial uncertainty level (the vertical width of the magenta lines). The uncertainty of the estimated pressure field slightly increases during the prediction step, before it decreases after an analysis step. This is a typical behaviour of a sequential assimilation system. More specifically, water breakthroughs are not observed in all production wells during the history matching period. The true reservoir pressure and saturation behaviour are well predicted and within the uncertainty level. Similar good results are obtained for the other injection and production wells.

Similar conclusions can be made from the results in the disconnected channel case as can be seen from Figs. 7 and 8 which are plotted in the same spirit of Figs. 5 and 6. During the first 192 days, the estimated log permeability field and facies pattern indicate a disconnected channel, but with a quite large uncertainty. The filter efficiently recovers the true fields in the last 608 days. The corresponding uncertainties further decreases over time and become much smaller than the initial uncertainties. Again, the history matched permeability field and facies pattern are almost identical to the truth at the end of the history matching period, and the truth lies within the uncertainties estimated by the filter. Fig. 7 further demonstrates that the estimated state of the disconnected channel reservoir are also quite good.

7.2. Two-Dimensional Closed Feature

For a two-dimensional closed feature, a typical realization of the state vector for the EnSRF will be of the same form as equation (26).

In practical applications, very often some prior information about the existence of a closed feature reservoir are available but not about the shape and location. We therefore generate an initial ensemble that reflects the reality of these problems, mainly having a closed features quite different than the true permeability field in term of shape and location. The discontinuous curve of the level set functions and the corresponding permeability fields for four realizations of the initial ensemble are presented in Fig. 9. The choice of the initial ensemble is also reflected in the log permeability and facies pattern plots on day 0 of Fig. 10.

As in the channel cases, Fig. 10 shows that the proposed history matching system is capable of recovering the basic structures of the true permeability field after 576 assimilation despite starting the estimation process from a very poor initial prior. The corresponding uncertainties further continuously decrease over time and are significantly less than the initial uncertainties at the end of the assimilation window. The final estimated permeability is almost the same as the true one, except at one cell located on the left boundary (and can be easily identified in the

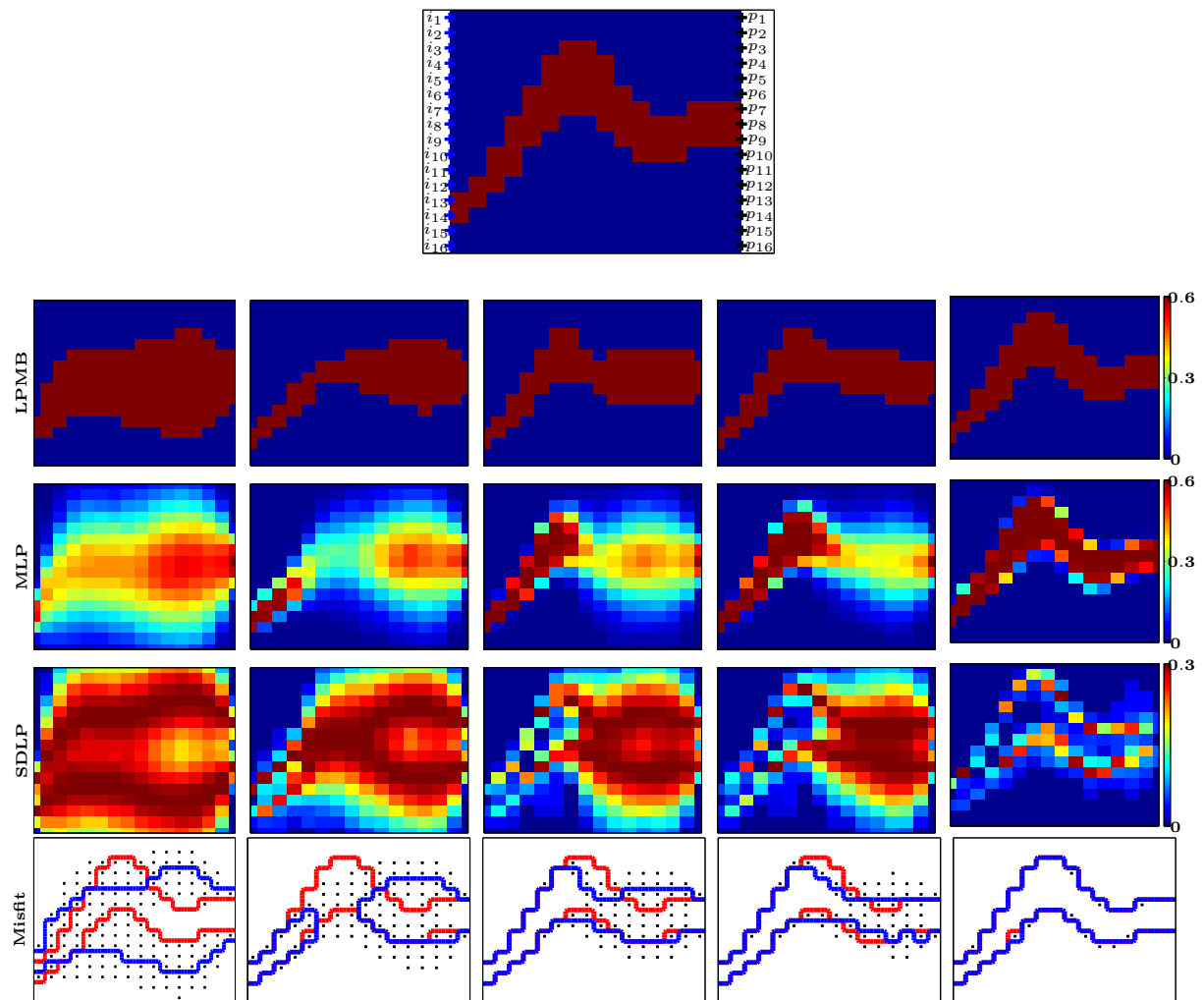


Figure 5. The true log permeability field (first row) and the log permeability field as estimated from the mean of the B-splines (second row), and mean (third row) and standard deviation (fourth row) of the log permeability field and misfit of facies pattern (fifth row) for the curved channel case. Results are shown at the end of 0^{th} , 192^{th} , 384^{th} , 576^{th} and 800^{th} days with 600 realization. For the true log permeability field, the injection well is plotted in blue pluses and the production wells in black pluses. The misfit figures show the true facies pattern (red), the estimated facies pattern (blue), and the cells with facies standard deviation greater than 0.8 (black dots).

misfit figure on day 800 of Fig. 11). At this location, the estimated field is quite different than the truth and lies outside the estimated uncertainty.

Fig. 11 shows the time-evolution of the assimilated processes in the injection well no. 7 and the three production wells no. 3, 14 and 16. Despite the facies mismatch in one of the cells, both history matching and predicting has been achieved very well. The typical behavior of the sequential assimilation system is also observed as before with an uncertainty increase after every prediction step before it gets corrected with the new observations with the Kalman filter analysis step. Similar good results are obtained for the other injection and production wells.

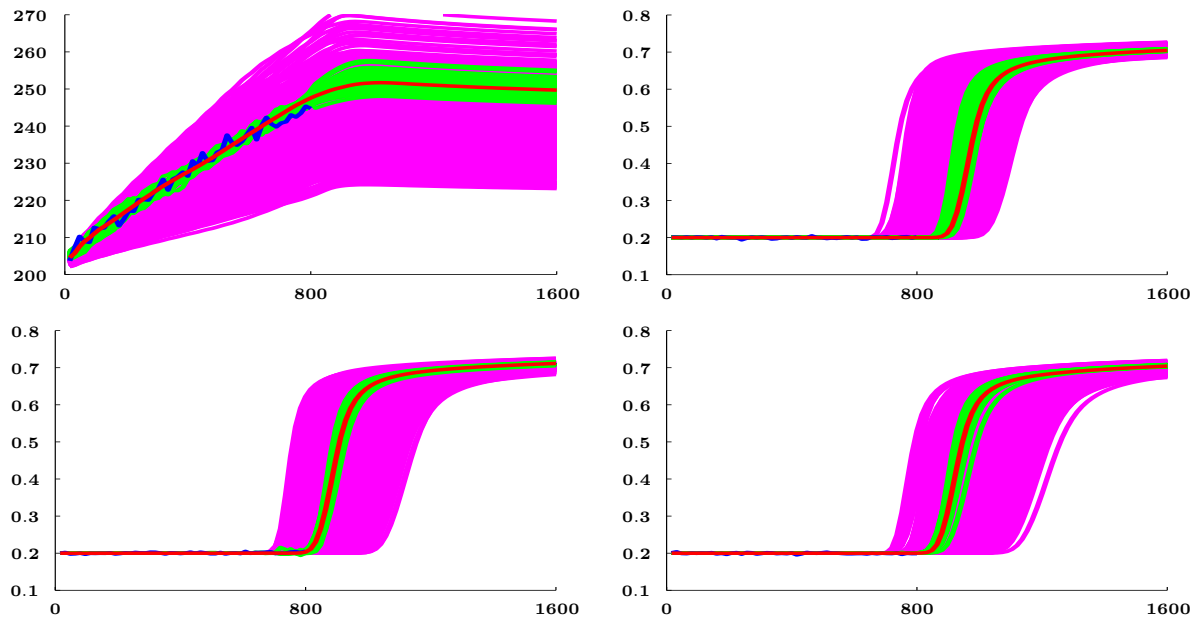


Figure 6. Time-evolution of the estimated pressure field in injection well no. 7 (top left) and saturation field (top right and bottom row) of production well no. 3, 14 and 16 over the production period for the case of a curved channel with 600 realization. The figure shows the true states (red), measurements (blue), simulations of the initial ensembles (magenta) and history matched ensembles (green).

7.3. Sensitivity to Ensemble Size

Application of the EnSRF to computationally demanding models incurs large computational costs for integrating the ensemble forward in time. This sets severe limits on the size of the ensemble that can be used in practice. However, an ensemble with few realizations can impair the performance of the filter analysis in realistic reservoir applications. Balance between the quality of the estimate and acceptable computing resources should be therefore found. Here, we test the assimilation system with a smaller ensemble size, conducting the same experiments as in sections 7.1 and 7.2 but using only 100 ensemble realizations. One may note that it takes a dual-core Macbook Unibody (P8800, 2.40GHz, 2G RAM) around 4 hours to complete the history matching process when the EnSRF is implemented with 100 realizations and around 23 hours with 600 realizations in Matlab.

Figs. 12-17 are plotted in the same spirit as Figs. 5-8, 10 and 11. One can see from Figs. 12, 14 and 16 that although the structure and the uncertainty of the initial ensemble are almost identical to the corresponding runs with 600 realizations, the evolution of the permeability estimation is very different. In contrast with the assimilation run with 600 realisations, the number of cells with larger facies uncertainty are reduced much faster using 100 realizations. At the end of the history matching period, the estimated permeability fields contain more mismatch cells compared to the estimates obtained with 600 realizations. In Figs. 13, 15 and 17, the uncertainty level (vertical width of the green lines) resulting from the EnSRF with 100 realizations is also much smaller than the one resulting using 600 realizations. The true pressure and saturation, however, lie within the uncertainty level in each well over most of the history matching period.

We consider three measures to quantify and better compare the results of the two runs:

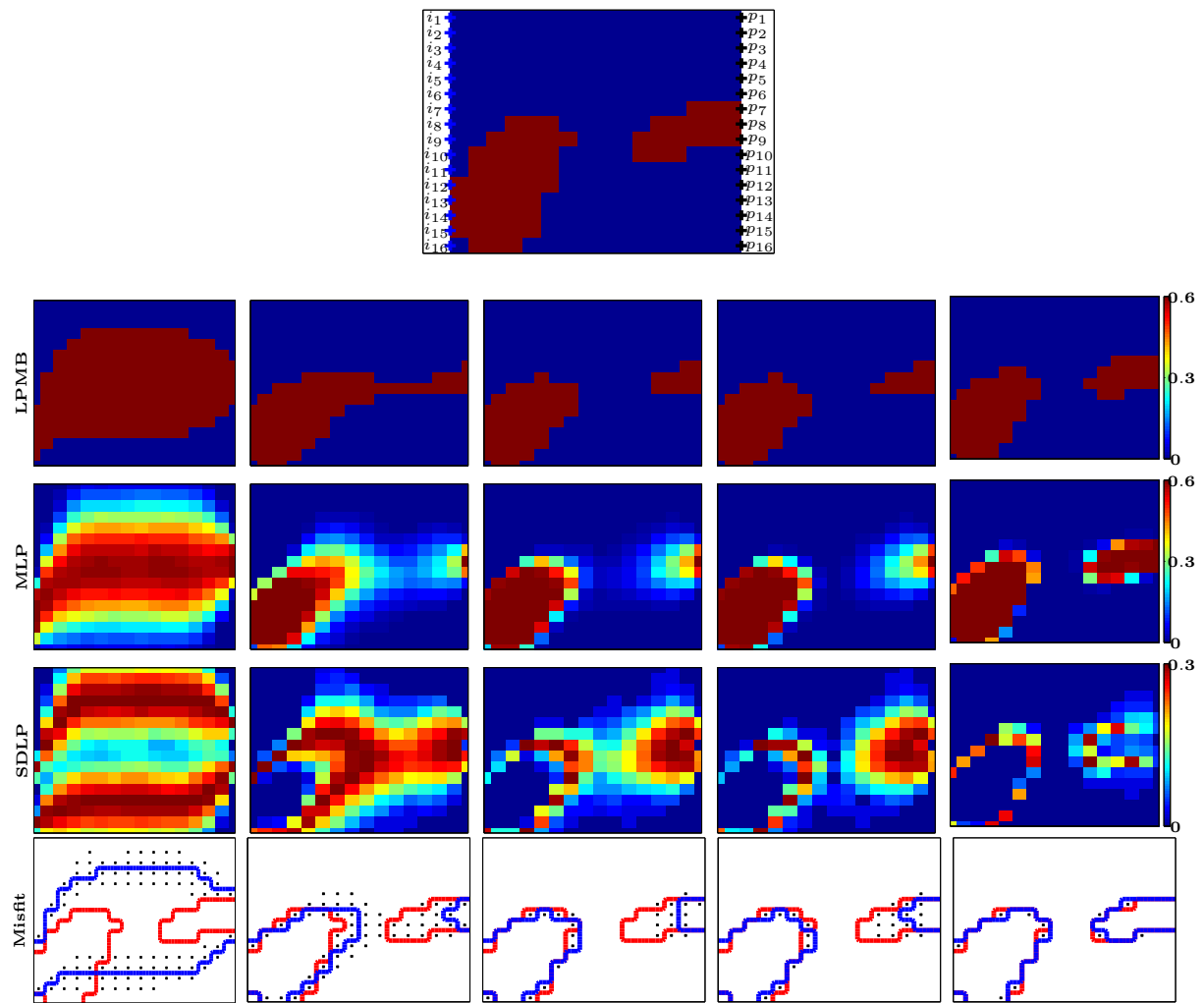


Figure 7. The true log permeability field (first row) and the log permeability field using the mean of the B-splines (second row) and mean (third row) and standard deviation (fourth row) of the log permeability field and misfit of facies pattern (fifth row) for the disconnected channel case. Results are shown at the end of 0^{th} , 192^{th} , 384^{th} , 576^{th} and 800^{th} days with 600 realization. For the true log permeability field, the injection well is plotted in blue pluses and the production wells in black pluses. The misfit figures show the true facies pattern (red), the estimated facies pattern (blue), and the cells with facies standard deviation greater than 0.8 (black dots).

- (i) *Permeability Mismatch:*
The number of cells in which the true permeability is different from the EnSRF estimate and lie outside the uncertainty level.
- (ii) *Pressure/Saturation Coverage:*
The total number of time steps for which the true pressure in all injection wells (or saturation in all production wells) lie within the estimated uncertainties level are calculated. This number is then divided by the number of injection (or production) wells and the total number of time steps to compute the percentage of pressure (or saturation) coverage.
- (iii) *Pressure/Saturation Average Uncertainty:*
The uncertainties (vertical width of the green lines in Figs. 6, 8, 11, 13, 15 and 17) of the

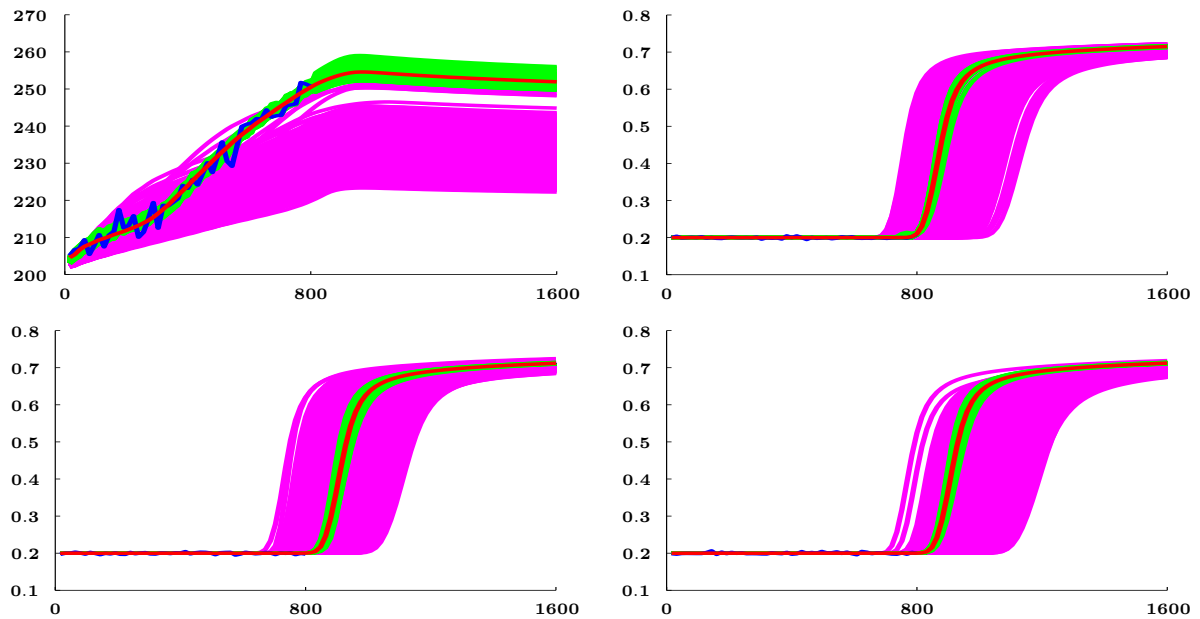


Figure 8. Time-evolution of the estimated pressure in injection well no. 7 (top left) and the saturation (top right and bottom row) of production well no. 3, 14 and 16 over the production period for the case of a disconnected channel with 600 realization. The figure shows the true states (red), measurements (blue), simulations of the initial ensembles (magenta) and history matched ensembles (green).

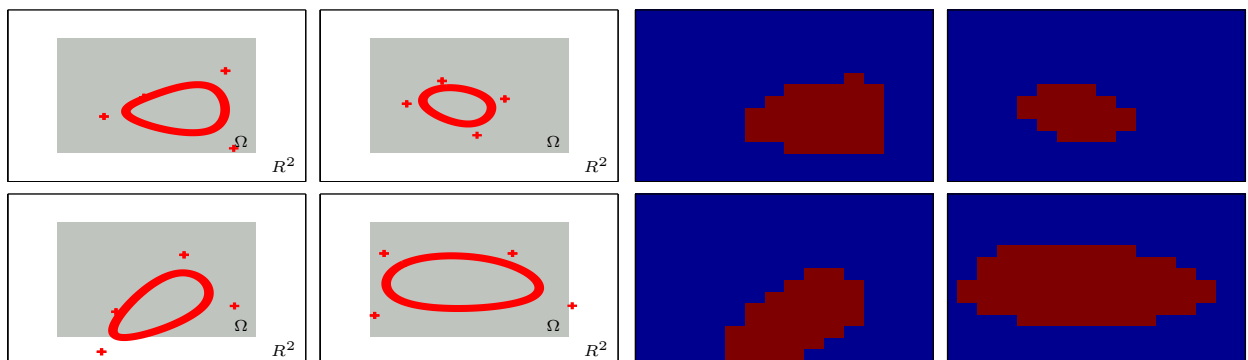


Figure 9. Four typical realizations of the initial ensemble for the case of the two-dimensional closed reservoir. In the left panels, the reservoir domain Ω is the grey rectangle, the B-spline control point domain is the outer white rectangle bounded by black edges, the B-spline control points are indicated in red pluses, the discontinuous curve of the level set function is the red curve). The right panels plot the corresponding permeability fields using equations (19 and 20).

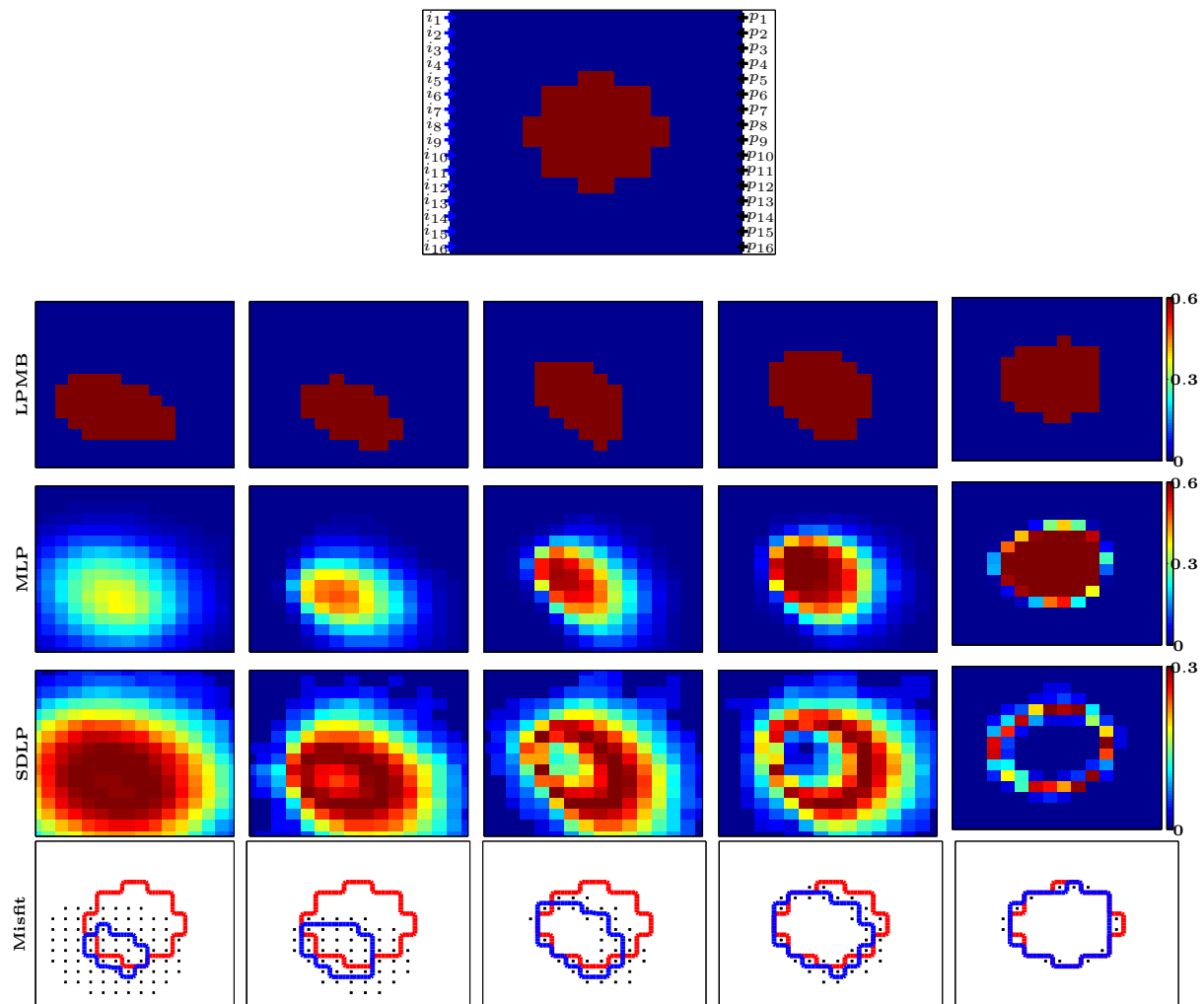


Figure 10. The true log permeability field (first row) and the log permeability field as estimated from the mean of the B-splines (second row), and mean (third row) and standard deviation (fourth row) of the log permeability field and misfit of facies pattern (fifth row) for the two-dimensional closed permeability case. Results are shown at the end of 0^{th} , 192^{th} , 384^{th} , 576^{th} and 800^{th} days with 600 realization. For the true log permeability field, the injection well is plotted in blue pluses and the production wells in black pluses. The misfit figures show the true facies pattern (red), the estimated facies pattern (blue), and the cells with facies standard deviation greater than 0.8 (black dots).

pressure in all injection wells (or saturation in all production wells) are calculated at each time step. The average uncertainty is then computed by averaging these uncertainties over the number of time steps and the number of injection wells (or production wells) .

Comparison results of these measures for the EnSRF runs with 100 and 600 realisations are presented in tables 2 and 3, respectively. In term of predicting the reservoir behaviour, both runs lead to very similar (perfect) results. This is because the data coverages in both cases are above 90%. However, in term of reservoir risk and management, EnSRF with 100 realizations significantly underestimates the pressure and saturation uncertainties in all the wells. For all three different reservoir types, the average pressure and saturation uncertainties are underestimated and are about half and third of the uncertainties estimated using 600 realizations,

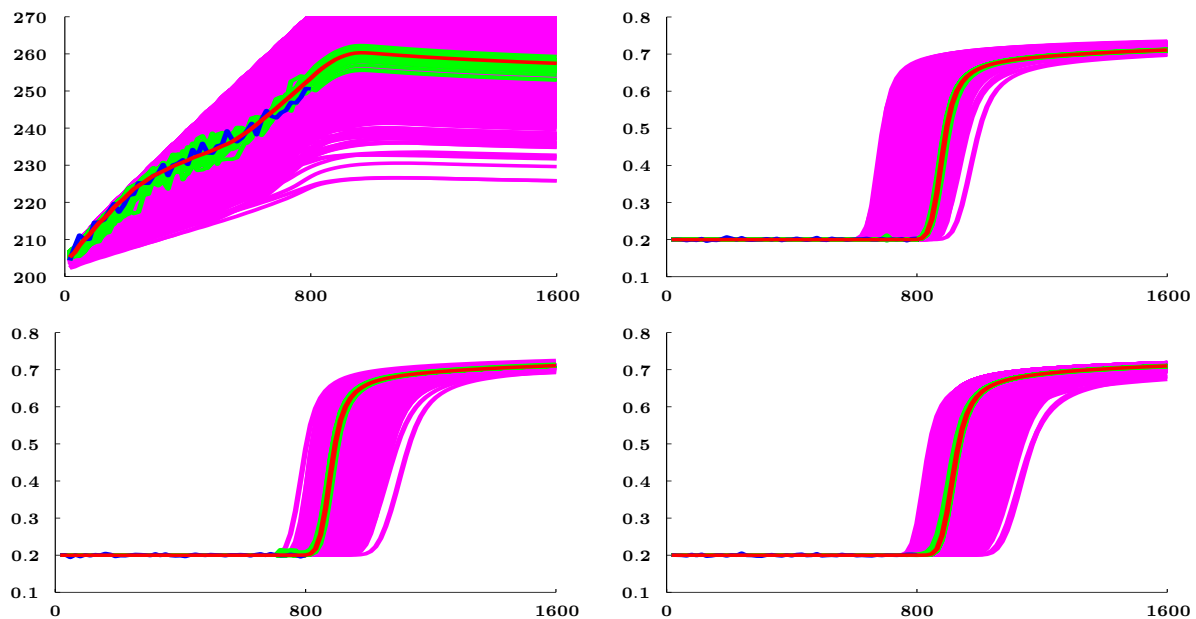


Figure 11. Time-evolution of the estimated pressure field in injection well no. 7 (top left) and saturation field (top right and bottom row) of production well no. 3, 14 and 16 over the production period for the case of two-dimensional closed permeability field with 600 realization. The figure shows the true states (red), measurements (blue), simulations of the initial ensembles (magenta) and history matched ensembles (green).

respectively. Concerning the quality of the permeability estimates, more mismatch cells results from the EnSRF were obtained using 100 realizations.

8. Conclusions

The aim of this paper is to develop an efficient method for using an ensemble Bayesian filter for the problem of history matching of facies pattern in a reservoir model - a problem of which a approach such as an conventional ensemble Kalman filter directly seeking the permeability and other fields might not be an appropriate choice. This is because the variable representing the facies is a discrete variable, and hence non-differentiable and non-Gaussian. By a proper representation of the permeability field using level set functions and a continuous B-spline parameterization, we transformed the history matching problem of the facies pattern to an estimation problem of continuous variables which can be treated by an ensemble Kalman filter. Here we used the ensemble square-root filter (EnSRF).

We conducted numerical experiments with three different types of reservoirs, with two facies types and complicated geological structure and assuming piecewise constant permeability profiles. Starting from vague priors, the new method efficiently recovered the true facies pattern at the end of the history matching period. The uncertainties of the estimated state variables conditional to the data were also substantially reduced compared to the initial uncertainties. The results of the different experiments demonstrate that the proposed method is robust and was able to provide accurate estimates of the reservoir structure. We also studied the the performance of our system using fewer ensemble realizations. Using ensembles of only 100 realizations, the EnSRF provided reasonable estimates of the reservoir state, but failed to accurately estimate the associated uncertainty and the permeability field. A larger ensemble size is then needed to better describe the distribution of the reservoir state vector (here we used 600 realizations).

		Reservoir Type		
		Connected Channel	Disconnected Channel	Closed Feature
Mismatch	Permeability	0	0	1
Coverage	Pressure	100%	100%	100%
	Saturation	100%	100%	100%
Average	Pressure (Bar)	6.03	4.65	5.13
Uncertainty	Saturation	0.0346	0.0267	0.0112

Table 2. Measures of the permeability mismatch, production data coverages, and average uncertainties as they result from the EnSRF using 600 realizations.

		Reservoir Type		
		Connected Channel	Disconnected Channel	Closed Feature
Mismatch	Permeability	9	3	2
Coverage	Pressure	99.8%	99.2%	99.8%
	Saturation	94.5%	90.3%	94.9%
Average	Pressure (Bar)	3.24	2.53	2.62
Uncertainty	Saturation	0.0132	0.00891	0.00498

Table 3. Measure of permeability mismatch, production data coverages, and average uncertainties as they result from EnSRF using 100 realizations.

Future work will further investigate this problem before considering more realistic reservoir applications. The experiments presented in this paper with an idealized reservoir problem were used to test the new method and to demonstrate its ability to tackle the history matching problem of reservoir facies.

9. Acknowledgement

The principal author, Lian Duan, thanks Mr. Yasin Abbas (Institute of Biomedical Engineering, University of Oxford) for technical help on the computational problems. This work was supported in part by Award No KUK-C1-013-04 from King Abdullah University of Science and Technology (KAUST).

References

- [1] Jafarpour B and McLaughlin D 2008 *Computational Geosciences* **12** 227–244
- [2] Williams M, Keating J and Barghouty M 1998 *SPE Reservoir Evaluation & Engineering* **1** 169–176
- [3] Agarwal B, Hermansen H, Sylte J and Thomas L 2000 *SPE Reservoir Evaluation & Engineering* **3** 534–543
- [4] Jahns H O 1966 *Soc. Petrol. Eng. J.* **237** 315–327
- [5] Farmer C 2005 *Mathematical Methods and Modelling in Hydrocarbon Exploration and Production* 119–212
- [6] Evensen G 1994 *Physica D* **77** 108–128
- [7] Evensen G 1994 *J Geophys Res* **99** 10,143–10,162
- [8] Oliver D 1996 *Mathematical Geology* **28** 811–817
- [9] Zhang F and Reynolds A Optimization algorithms for automatic history matching of production data *8th European Conference on the Mathematics of Oil Recovery*
- [10] Zhang F, Skjervheim J, Reynolds A and Oliver D 2005 *SPE Reservoir Evaluation & Engineering* **8** 214–223
- [11] Oliver D S, Reynolds A C, Bi Z and Abacioglu Y 2001 *Petroleum Geosciences* **7** 65–73
- [12] Oliver D and Chen Y 2010 *Computational Geosciences* **15** 185–221
- [13] Reading H 1996 *Sedimentary environments: processes, facies, and stratigraphy* (Wiley-Blackwell)
- [14] Tai X c and Yao C h 2006 *J. Comput. Math.* **24** 435–443
- [15] Sethian J A 1999 *Level set methods and fast marching methods* vol 3 (Cambridge: Cambridge University)

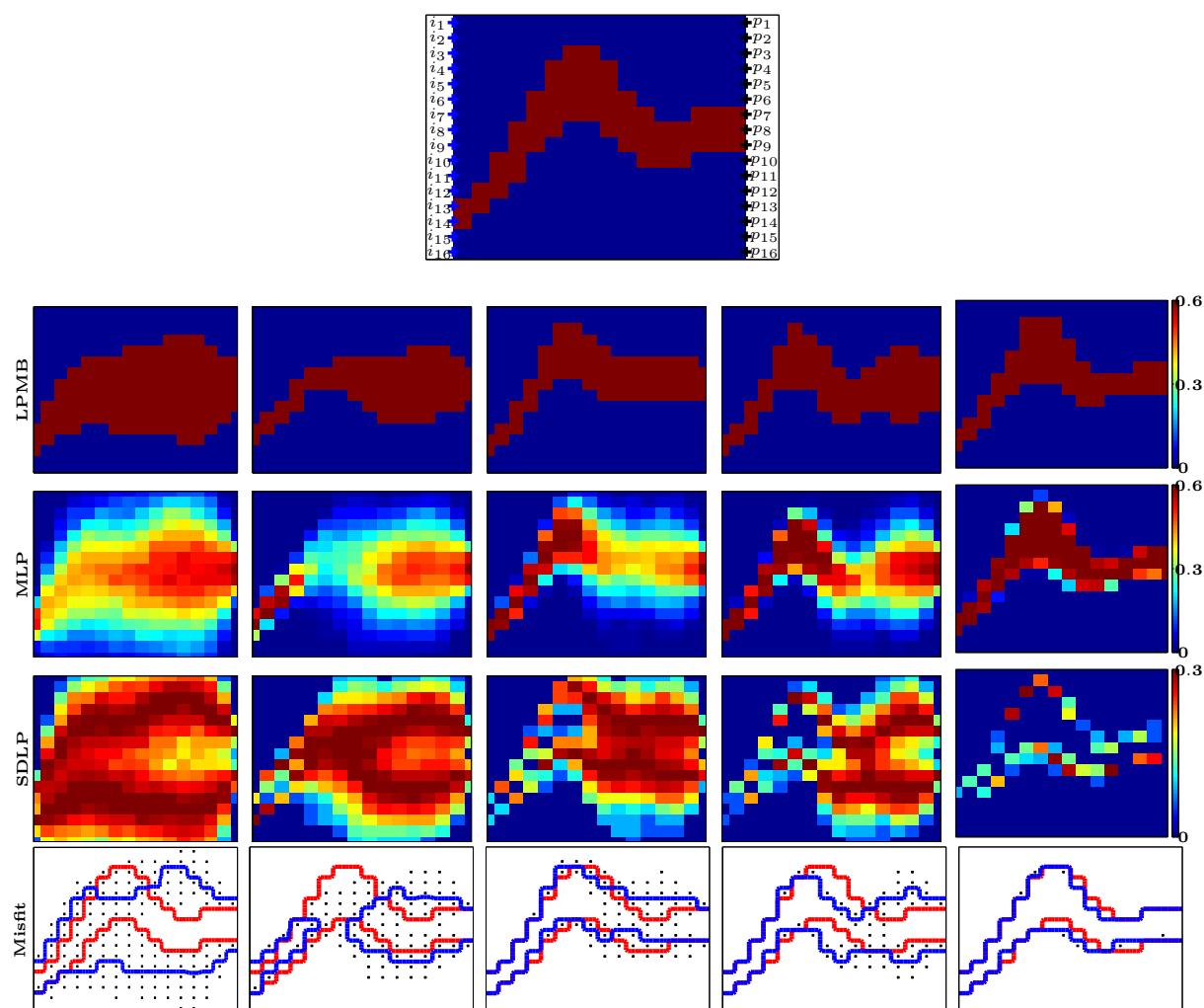


Figure 12. The true log permeability field (first row) and the log permeability field as estimated from the mean of the B-splines (second row), and mean (third row) and standard deviation (fourth row) of the log permeability field and misfit of facies pattern (fifth row) for the mountain-shaped channel case. Results are shown at the end of 0^{th} , 192^{th} , 384^{th} , 576^{th} and 800^{th} days with 100 realization. For the true log permeability field, the injection well is plotted in blue pluses and the production wells in black pluses. The misfit figures show the true facies pattern (red), the estimated facies pattern (blue), and the cells with facies standard deviation greater than 0.8 (black dots).

Press) evolving interfaces in computational geometry, fluid mechanics, computer vision, and materials science

- [16] Tsai R and Osher S 2003 *COMM.MATH.SCI* **1** No. 4 623–656
- [17] Chan T F and Tai X C 2003 *J.Comput.Physics* **193** 40–66
- [18] Chan T and Vese L A 2001 *IEEE Tran. image Proc.* **10** 266–277
- [19] Wang S Y, Lim K M, Khoo B C and Wang M Y 2007 *J. Comput. Phys.* **221** 395–421
- [20] Nielsen L, Li H, Tai X, Aanonsen S and Espedal M 2010 *Computing and visualization in science* **13** 41–58
- [21] Dorn O and Villegas R 2008 *Inverse Problems* **24** 035015
- [22] Han X and Li X 2008 *Remote Sensing of Environment* **112** 1434–1449
- [23] Whitaker J S and Hamill T M 2002 *Monthly Weather Review* **130** 1913–1924
- [24] Liu N and Oliver D 2005 *Journal of Petroleum Science and Engineering* **47** 147–161

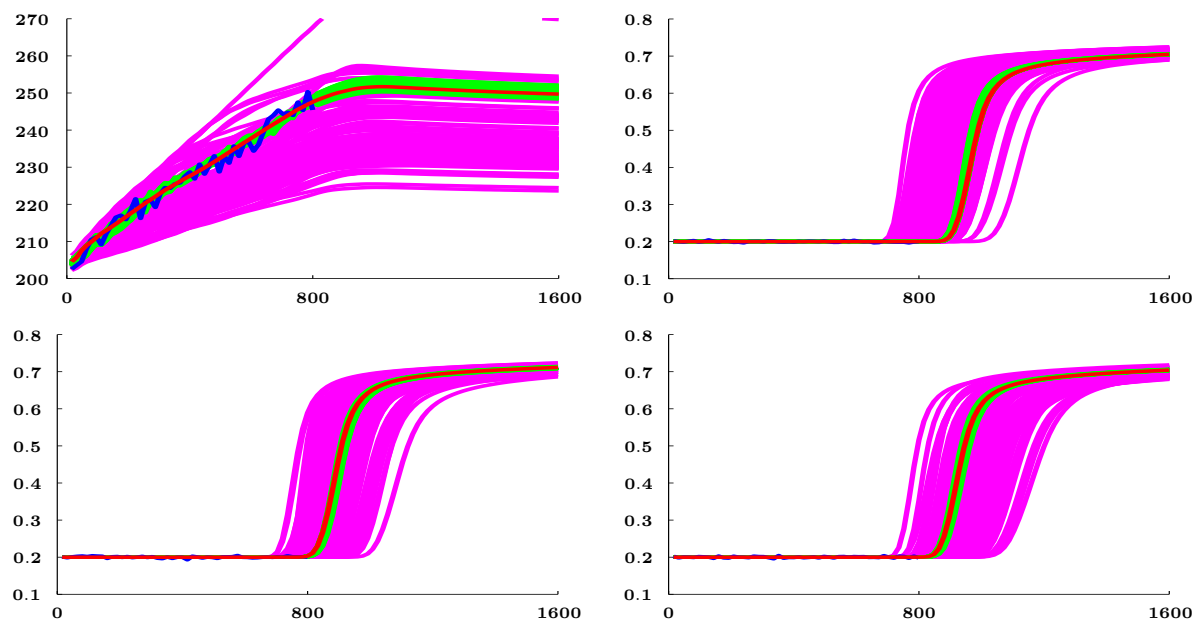


Figure 13. Time-evolution of the estimated pressure field in injection well no. 7 (top left) and saturation field (top right and bottom row) of production well no. 3, 14 and 16 over the production period for the case of a connected channel with 100 realization. The figure shows the true states (red), measurements (blue), simulations of the initial ensembles (magenta) and history matched ensembles (green).

- [25] Liu N and Oliver D 2005 *SPE Reservoir Evaluation and Engineering* **8(6)** 470–477
- [26] Chang H, Zhang D and Lu Z 2010 *Journal of Computational Physics* **229** 8011–8030
- [27] Ren H, Wu Y and Zhu X 2006 *Journal of Forestry Research* **17** 150–152
- [28] Tustison N, Avants B and Gee J Improved ffd b-spline image registration *IEEE 11th International Conference on Computer Vision* (IEEE) pp 1–8
- [29] Liu X, Huang H and Xu W 2005 *Computational Science/ICCS 2005* 995–1002
- [30] Mora M, Andrade J and Tauber C Regularized multilevel b-spline registration: Application to cardiac motion estimation *IEEE international conference on Biomedical imaging: from nano to Macro* (IEEE) pp 512–515
- [31] Brouwer D R, Naedal G, Jansen J D, Vefring E H and van Kruijsdijk C P J W 2004 *SPE* 90149
- [32] Naedal G, Mannseth T and Vefring E H 2002 *SPE-75235*
- [33] Prautzsch H, Boehm W and Paluszny M 2002 *Bzier and B-spline techniques* (Springer Verlag)
- [34] Gavalas G, Shah P and Seinfeld J 1976 *Old SPE Journal* **16** 337–350
- [35] Tarantola A 2004 *Inverse Problem Theory. Methods for Model Parameter Estimation* Philadelphia, PA:SIAM

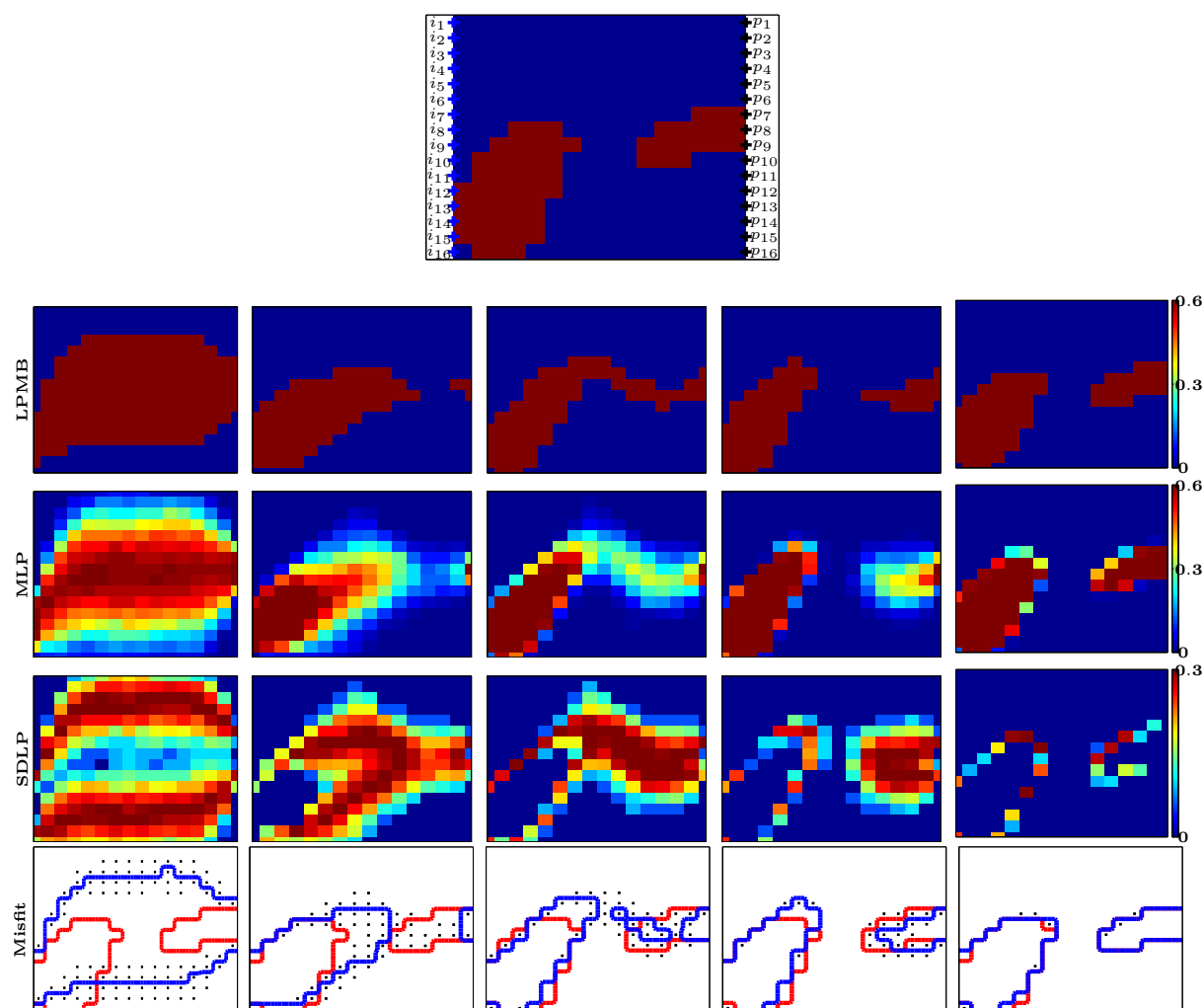


Figure 14. The true log permeability field (first row) and the log permeability field using the mean of the B-splines (second row) and mean (third row) and standard deviation (fourth row) of the log permeability field and misfit of facies pattern (fifth row) for the disconnected channel case. Results are shown at the end of 0th, 192th, 384th, 576th and 800th days with 100 realization. For the true log permeability field, the injection well is plotted in blue pluses and the production wells in black pluses. The misfit figures show the true facies pattern (red), the estimated facies pattern (blue), and the cells with facies standard deviation greater than 0.8 (black dots).

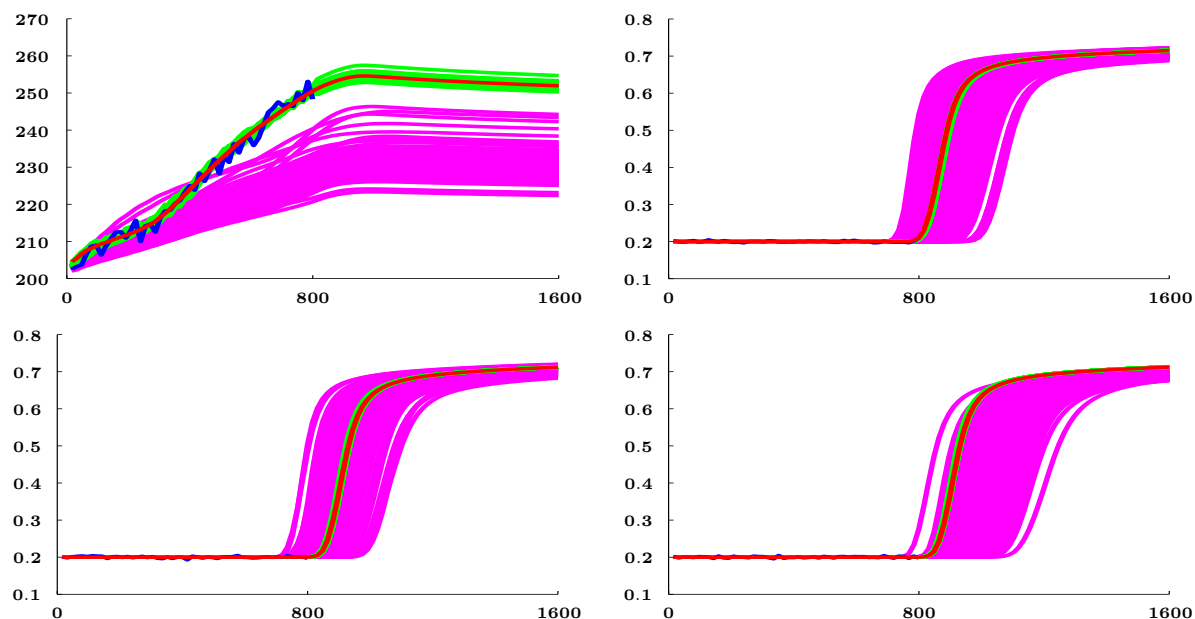


Figure 15. Time-evolution of the estimated pressure in injection well no. 7 (top left) and the saturation (top right and bottom row) of production well no. 3, 14 and 16 over the production period for the case of a disconnected channel with 100 realization. The figure shows the true states (red), measurements (blue), simulations of the initial ensembles (magenta) and history matched ensembles (green).

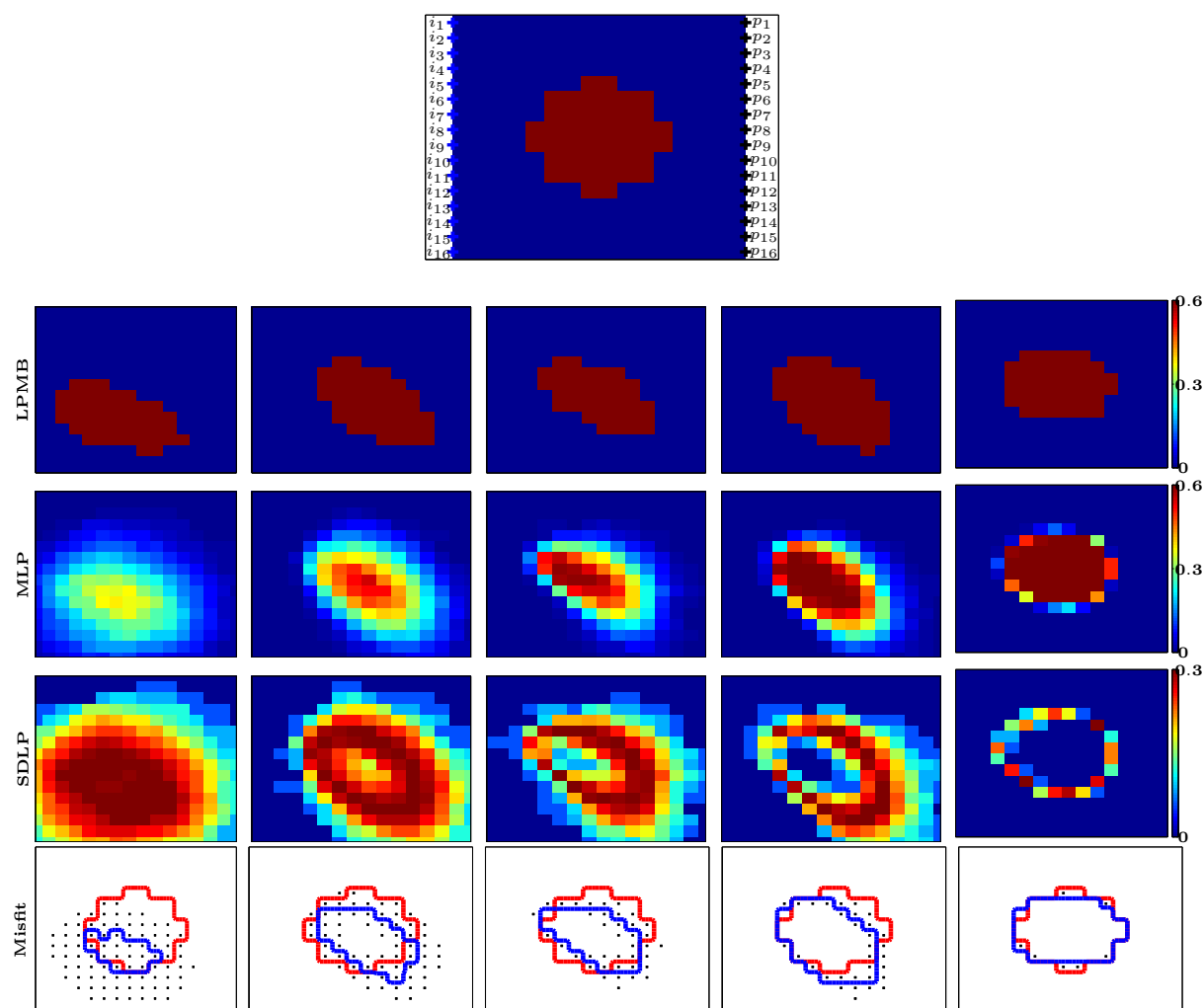


Figure 16. The true log permeability field (first row) and the log permeability field as estimated from the mean of the B-splines (second row), and mean (third row) and standard deviation (fourth row) of the log permeability field and misfit of facies pattern (fifth row) for the two-dimensional closed permeability case. Results are shown at the end of 0^{th} , 192^{th} , 384^{th} , 576^{th} and 800^{th} days with 100 realization. For the true log permeability field, the injection well is plotted in blue pluses and the production wells in black pluses. The misfit figures show the true facies pattern (red), the estimated facies pattern (blue), and the cells with facies standard deviation greater than 0.8 (black dots).

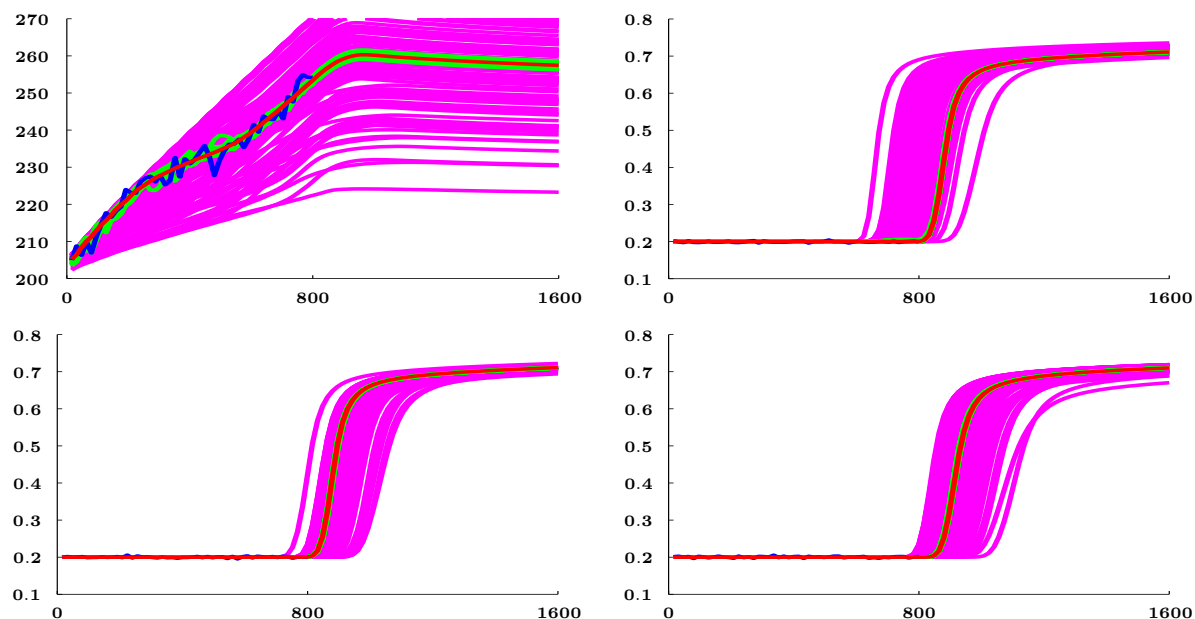


Figure 17. Time-evolution of the estimated pressure field in injection well no. 7 (top left) and saturation field (top right and bottom row) of production well no. 3, 14 and 16 over the production period for the case of two-dimensional closed permeability field with 100 realization. The figure shows the true states (red), measurements (blue), simulations of the initial ensembles (magenta) and history matched ensembles (green).